Mon. Not. R. Astron. Soc. **000**, 1–?? (2014) Printed 22 December 2014 (MN LATEX style file v2.2)

Modeling Complex Organic Molecules in dense regions: Eley-Rideal and complex induced reaction

M. Ruaud[12⋆], J. C. Loison [34†], K. M. Hickson [34], P. Gratier [12], F. Hersant [12], V. Wakelam [12]
[1]*Univ. Bordeaux, LAB, UMR 5804, F-33270, Floirac, France*
[2]*CNRS, LAB, UMR 5804, F-33270, Floirac, France*
[3]*Univ. Bordeaux, ISM, UMR 5255, F-33400 Talence, France*
[4]*CNRS, ISM, UMR 5255, F-33400 Talence, France*

arXiv:1412.6256v1 [astro-ph.SR] 19 Dec 2014

Accepted 2014 December 18. Received 2014 December 18; in original form 2014 November 17

ABSTRACT
Recent observations have revealed the existence of Complex Organic Molecules (COMs) in cold dense cores and prestellar cores. The presence of these molecules in such cold conditions is not well understood and remains a matter of debate since the previously proposed "warm-up" scenario cannot explain these observations. In this article, we study the effect of Eley-Rideal and complex induced reaction mechanisms of gas-phase carbon atoms with the main ice components of dust grains on the formation of COMs in cold and dense regions. Based on recent experiments we use a low value for the chemical desorption efficiency (which was previously invoked to explain the observed COM abundances). We show that our introduced mechanisms are efficient enough to produce a large amount of complex organic molecules in the gas-phase at temperatures as low as 10K.

Key words: astrochemistry – ISM: abundances – ISM: clouds – molecules

1 INTRODUCTION

Complex Organic Molecules (COM here after), such as CH_3OH, CH_3CHO, $HCOOCH_3$ and CH_3OCH_3 (see Herbst & van Dishoeck 2009, for a review), have long been observed in hot cores or hot corinos of warm star-forming regions such as SgB2 (Cummins et al. 1986), OMC-1 (Blake et al. 1987) or IRAS 16293-2422 (Bottinelli et al. 2004). Although some of these molecules such as CH_3OH and CH_3CHO were also observed in cold environments like the TMC-1 or L134N dark clouds (Matthews et al. 1985; Friberg et al. 1988), a search for more complex COMs dimethyl ether yielded only upper limits (Friberg et al. 1988). In the B1-b dense core, Öberg et al. (2010) reported detections of CH_3OH, CH_3CHO, $HCOOCH_3$ and tentatively detected CH_3OCH_3. Recently, Cernicharo et al. (2012) reported the discovery of the methoxy radical (CH_3O) in this source. Furthermore, observations conducted by Bacmann et al. (2012) have revealed the existence of a variety of COMs in the cold prestellar core L1689b and more recently toward the prestellar core L1544 (Vastel et al. 2014). From these detections, new challenges arise for current chemical models. Indeed, in star forming regions, these COMs are thought to be formed via recombination of radicals, at temperatures around 30K, on ices during the warm-up period which are then released into the gas-phase at temperatures above 100K (Garrod & Herbst 2006). In cold cores which are characterized by a very low temperature (∼10K), this mechanism cannot explain the observed abundance of such molecules.

Recently, Vasyunin & Herbst (2013), have proposed that these complex species are formed via gas phase ion-molecular and neutral-neutral chemistry from precursors such as formaldehyde and methanol. In this scenario, these precursors are formed on icy grain surfaces thanks to the surface mobility of atoms such as hydrogen, oxygen and nitrogen. These precursors are then released to the gas-phase via efficient reactive desorption (i.e ∼ 10% of the newly formed species desorb) (Garrod et al. 2007). The proposed scenario leads to reasonable results at temperature as low as 10K for a range of molecules. However the reactive desorption mechanism is not a fully understood process. Recent experiments conducted by Minissale & Dulieu (2014) showed that this process may not be as efficient as previously thought (see discussion in Section 2.1). It is important to note that thermal and cosmic ray induced desorption mechanisms are unable to reproduce the observed COM abundances in their simulations.

In this article, we propose an alternative/complementary scenario, in which Eley-Rideal and the complex induced reaction mechanisms on grain surfaces modify the chemical reactivity and can be efficient under some conditions to reproduce the observed COM abundances in cold and dense regions. Indeed, usual gas-grain models consider that atoms and molecules present in the gas-phase may stick on interstellar dust grains through collisions. These species are only weakly bound to the surface (physisorbed), considering in most cases a sticking probability equal to 1 (Hasegawa

⋆ E-mail: ruaud@obs.u-bordeaux1.fr
† E-mail: jean-christophe.loison@u-bordeaux.fr

et al. 1992). These species can then react through the Langmuir-Hinshelwood mechanism (i.e. diffusion process).

In most astrophysical models, Eley-Rideal (atom or molecule reacting directly with adsorbed species) mechanisms are neglected considering the low density of reactive species on grains. This may be not the case for carbon atom collisions with interstellar ices as carbon atoms show high reactivity with most of the molecules adsorbed on grain surfaces and are present in the gas phase at high abundances.

Another critical point is the strength of the adsorption itself. In current astrochemical models the adsorption energy of a carbon atom on ice is taken to be 800 K (Hama & Watanabe 2013). This value has neither been measured nor calculated and could be significantly underestimated as ab-initio calculations lead to a binding energy of the C...H_2O van der Waals complex equal to 3600 K (Schreiner & Reisenauer 2006; Hwang et al. 1999; Ozkan & Dede 2012) and to a binding energy of the C...CH_3OH van der Waals complex equal to 8400 K (Dede & Ozkan 2012). Then, even if carbon atoms have been shown to react quickly with methanol in the gas phase (Shannon et al. 2013), the strength of the C...CH_3OH complex may prevent reaction if the energy dissipation is efficient enough to stabilize the complex.

This paper is organized as follows. In Section 2, we describe our chemical model and we introduce the basics of the considered mechanisms. In Section 3, we present the effect of Eley-Rideal and complex induced reaction mechanisms on our models and on the formation of COMs. In Section 4, we compare our modeling results with the observed COM abundances in B1-b and L1689b cold dense cores and L1544 prestellar core, showing that these processes play a significant role in reproducing the observed abundances. Finally, Section 5 contains a general discussion and a summary of our work.

2 CHEMICAL MODEL

2.1 The gas-grain code

For this work, we used the full gas-grain chemical model NAUTILUS described in Semenov et al. (2010) and Reboussin et al. (2014). This model is adapted from the original gas-grain model of Hasegawa et al. (1992) and its subsequent evolutions made over the years at Ohio State University. In this model, the abundance of each species is computed by solving a set of rate equations for gas-phase and grain-surface chemistries. Gas-phase and grain-surface chemistries are connected via accretion and desorption. Because of the low grain temperature expected in cold dense cores, we only consider physisorption. Desorption can be thermal, induced by stochastic cosmic ray heating or via the exothermicity of surface reactions. The rate at which surface bound species thermally desorb follows a Boltzmann law at the dust temperature (Hasegawa et al. 1992). The cosmic ray induced desorption is treated following Hasegawa & Herbst (1993) and the corresponding rate is given by:

$$k_{crd}(i) = f(70\mathrm{K})k_{des}(i, 70\mathrm{K}) \quad (1)$$

where $f(70\mathrm{K})$ is the fraction of the time spent by grains at 70K which is estimated to be $\sim 3.16 \times 10^{-19}$ for a cosmic ionization rate $\zeta_{\mathrm{H_2}} = 1.3 \times 10^{-17}$ s^{-1} and $k_{des}(i, 70\mathrm{K})$ the rate of thermal desorption for a grain at T_{dust}=70K. The desorption by exothermicity of surface reactions is treated following Garrod et al. (2007). In this scenario, for each surface reaction that leads to a single product, we consider that a part of the energy released during the reaction could contribute to break the surface-molecule bond. The fraction f of reactions resulting in desorption is calculated by modeling the competition between the rate of desorption and the rate of energy lost to the grain:

$$f = \frac{\nu P}{\nu_s + \nu P} = \frac{aP}{1 + aP} \quad (2)$$

where $a = \nu/\nu_s$, the ratio of the surface-molecule bond frequency to the energy at which energy is lost to the grain surface. P gives the probability of desorption and follows the Rice-Ramsperger-Kessel (RRK) theory (see Garrod et al. 2007, and references therein for more information). The value a is not well constrained but could be in the range of ∼0.0 (no chemical desorption) to ∼0.1 (high efficiency). However, recents experiments conducted by Minissale & Dulieu (2014) on the efficiency of the reactive desorption of the oxygen system (i.e. system with two open channels leading to O_2 and O_3) on oxidized graphite showed that this process is highly dependent on the surface coverage and linearly decreases with increasing surface coverage. They explain this phenomenon saying that the presence of a pre-adsorbed species possibly enhances the probability for the newly formed excited molecules to dissipate their excess energy, presumably making the chemical desorption process inefficient when the grain coverage is important.

Therefore, under these conditions, we choose to use a moderate value for the reactive desorption efficiency. We considered a value of $a = 0.01$, which is equivalent to consider that $\sim$ 1% of the newly formed species desorb at formation and $\sim$ 99% remain on the grain surface (see Garrod et al. 2007).

The surface chemistry is treated assuming that the ice mantle surrounding the interstellar grain core can be represented as an isotropic lattice with periodic potential. The width of barrier between two adjacent binding sites is set to 1Å and the height E_b of the barrier against diffusion is assumed to be 0.5× E_D (Garrod & Herbst 2006), where E_D is the desorption energy of the species. Atoms and molecules can diffuse on the grain surface by thermal hopping and then react with each other, according to Hasegawa et al. (1992) (we do not take into account diffusion by quantum tunneling in this study).

We also assume the "encounter desorption" process proposed by Hincelin et al. (2014) for grain surface molecular hydrogen. The determination of the H_2 coverage on a dust grain is critical due to the very different binding energies involved depending on whether H_2 adsorbs on water substrate (E_D=440K) or on H_2 substrate (E_D=23K)(Cuppen & Herbst 2007). Since H_2 is the most abundant species in the gas phase and because s-H_2O (water molecule on surface) is thought to be the main component of the ice mantle, the use of a single binding energy for H_2 can lead to very different results depending on the assumptions made. Indeed, considering that H_2 adsorbate on a water substrate can lead, at high density, to the formation of several H_2 monolayers on grain surfaces, is physically unacceptable considering the very low binding energy of H_2 on itself. In contrast, considering the binding energy of H_2 on itself prevents the adsorption of H_2 onto grain surfaces, which is not satisfactory at low temperature. The proposed approach by Hincelin et al. (2014) is based on the facile desorption of molecular hydrogen when it is adsorbed on an H_2 substrate and deals with these two binding energies. This method leads to reasonable results with a microscopic Monte Carlo stochastic method.

Finally, grains are considered to be spherical with a 0.1μm radius, a 3 g.cm^{-3} density and $\sim 10^6$ surface sites, all chemically active. The dust to gas mass ratio is set to 0.01.

2.2 The new chemical network

For this study, to calculate the various desorption rates, and the diffusive reaction rates, we used the binding energies E_D from Garrod & Herbst (2006). We adopted the gas-phase network *kida.uva.2011* with updates from Loison et al. (2012), Wakelam et al. (2013) and Loison et al. (2014). The grain network is based on Garrod et al. (2007). The grain surface network has been modified in order to include the new surface mechanisms (formation of van der Waals complexes and low temperature Eley-Rideal mechanisms). Several new species have been added to the model (see Table 2; adopted binding energies are also reported with their respective references) together with the reactions involving those species in the gas phase. The new mechanisms are described in section 2.2.1 and the new reactions are listed in Tables A1 and A2 of Appendix A. The full network is available at `http://kida.obs.u-bordeaux1.fr/models`.

2.2.1 Chemistry

In this study, we consider that when gas-phase carbon atoms land on grain surfaces they can either react directly (i.e. Eley-Rideal mechanism, C + s-X → s-CX) or form van der Waals complexes (C + s-X → s-C...X) with the main constituent molecules present on interstellar grains (i.e. s-X = s-H_2O, s-CO, s-NH_3, s-CO_2, s-CH_4, s-H_2CO and s-CH_3OH, see Fig. 1) or simply be physisorbed.

We consider that when there is no barrier for reaction, the C + s-X reaction occurs via the Eley-Rideal mechanism. This is the case for reactions C + H_2, C + CO and C + H_2CO which have no barrier (Harding 1983; Harding et al. 1993; Husain & Kirsch 1971; Husain & Ioannou 1999). On the other hand, for reactions such as C + s-H_2O, C + s-CO_2, C + s-NH_3, C + s-CH_4 and C + s-CH_3OH, we consider that atomic carbon will preferentially form a complex due to the presence of a deep van der Waals complex well. Consequently they will not react except through tunneling assuming that the height of the barrier is relatively unaffected by the presence of ice. This latter approximation is rather uncertain (Bromley et al. 2014) but has been shown to be valid for some systems using theoretical calculations: O + CO (Talbi et al. 2006), H + HOCCOH (Woods et al. 2013), H + H_2CO (Goumans 2011). Moreover, as the van der Waals energies are large, we consider that the s-C...X complexes are unable to move on the surface (see Table 2).

When a van der Waals complex is formed, atomic carbon will react with the highly mobile H atoms through reactions: s-C...X + s-H. The products of these reactions is energized s-CH...X radicals (e.g. internal energy for the CH...H_2O complex of ∼ 358 kJ/mol corresponding to the value of the exothermicity of the C + H → CH reaction added to the difference of C...H_2O (Schreiner & Reisenauer 2006; Hwang et al. 1999; Ozkan & Dede 2012) and CH...H_2O (Bergeat et al. 2009) van der Waals bond strengths). Considering the large value of the CH internal energy, energy dissipation is unlikely to be efficient enough to stabilize the CH...ice complex (see Table 2). We therefore consider that a small fraction of the CH radicals will desorb (i.e. 1%), another small fraction (i.e. 1%) will remain in the form of the CH...X complex and that most will react with the species X leading to more complex molecules. The reactions s-C...X + s-H → s-CH...X → s-Y are considered to have no barrier similary to the gas-phase for most of the CH reactions (Hickson et al. 2013; Canosa et al. 1997; Bocherel et al. 1996). The different reactions and products (with branching ratios) are given in Table A1 of Appendix A.

The products of surface reactions are usually considered to be adduct formation and the bimolecular exit channels are neglected given the fast energy dissipation (equivalent to a gas phase reaction with infinite pressure). For example, the s-CH + s-CH_4 reaction is assumed to lead only to s-C_2H_5 and not to s-C_2H_4 + s-H. This approximation is almost systematically used in current astrophysical models of grain chemistry and has yet to be verified by theoretical calculations. Nevertheless, it is likely to be a poor assumption for reactions where the bimolecular exit channel is very exothermic involving a low exit barrier. A good example is the s-CH + s-CO_2 reaction leading to s-HCOCO adduct formation which may partly fall apart to give s-HCO + s-CO. Even if s-CO and s-HCO remain relatively close together on the ice, they will lose their internal and kinetic energies through interaction with the surface preventing reformation of the s-HCOCO adduct which probably presents a notable barrier. The reactions of atomic species such as N, O with H on interstellar ices will also result in the formation of other highly energetic hydride species reagents. In the case of atomic nitrogen, the resulting s-NH and s-NH_2 radicals could then possess a significantly increased reactivity with respect to their ground state counterparts. However, as s-NH and s-NH_2 both show large to very large barriers for reactions with s-H_2O, s-CO, s-CO_2, s-CH_3OH, s-CH_4 and s-H_2CO, we currently neglect these reactions (Röhrig & Wagner 1994; Cohen & Westberg 1991).

The case of energized OH (formed by the O + H addition) is different. OH radicals show a high reactivity with CH_3OH (Jimnez et al. 2003; Xu & Lin 2007; Shannon et al. 2013) and H_2CO (Yetter et al. 1989; Xu et al. 2006) leading to H atom abstraction and then to CH_3O and HCO radicals and water. As s-CH_3O and s-HCO radicals will mainly react with the highly mobile s-H atoms on the surface, reforming s-CH_3OH and s-H_2CO, the main global reaction is s-OH + s-H → s-H_2O. The only specific case is when an O atom is bound to a CO molecule on the ice surface, s-O...CO, as energized OH formed by the s-O...CO + s-H reaction may react with s-CO to form s-HOCO. Indeed the OH + CO → HOCO reaction shows a very small barrier (Fulle et al. 1996; Joshi & Wang 2006; Nguyen et al. 2012). The energized HOCO adduct may then fall apart further to yield H + CO_2 as shown in a recent H_2O-CO ice photodissociation experiment (Arasa et al. 2013). We introduce the s-O...CO van der Waals complex and HOCO in the model. We performed DFT calculations showing that HOCO reacts with H atoms without a barrier, producing formic acid (HCOOH) or H_2 + CO_2 through direct H atom abstraction (in good agreement with Yu & Francisco 2008; Dibble & Zeng 2010). In their H_2O-CO ice photodissociation study, Arasa et al. (2013) calculated that most of the OH is relaxed, 3% of OH radicals lead to HOCO formation and only 0.036% lead to CO_2 + H formation. However in their case the OH formed by H_2O photodissociation had an average OH internal energy estimated to be equal to 68 kJ/mol, much smaller than in the case of OH formation from the O + H addition reaction (430 kJ/mol). We consider that energized OH from the s-O...CO + s-H addition leads to 1% of OH desorption, 20% of OH relaxation, 19% to s-HOCO formation and 60% to s-H + s-CO_2 formation. For the s-H + s-HOCO reaction, we consider that 10% of reactive events lead to s-HCOOH formation, 19% to s-H_2O + s-CO with the other 70% leading to s-H_2 + s-CO_2 formation. As already mentioned, in the case of energized CH, we assume only 1% of relaxation, compared to a value of 20% for the equivalent energized OH formation process. The reason for this assumption is that the van der Waals complexes of atomic carbon are generally much stronger than those of oxygen atoms (O...CO stabilization is calculated equal to 258 K (Goumans & Andersson 2010)) so that carbon atom complexes are characterized by shorter van der Waals distances. As a result, en-

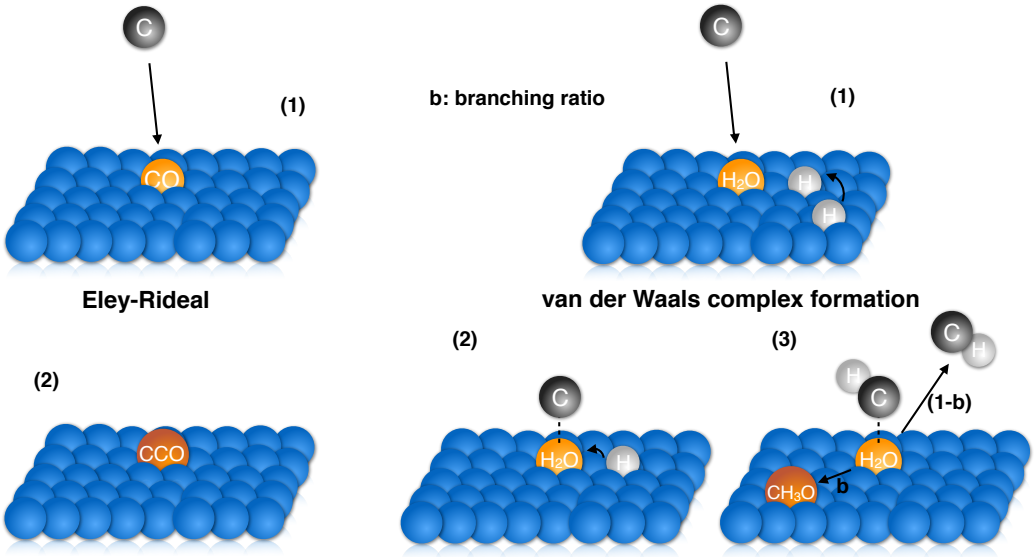

Figure 1. Sketch illustrating the Eley-Rideal and complex induced reaction mechanisms on grain surfaces.

Table 1. Summary of grain surface processes considered in this study

Reaction†			Assumptions and comments
C + s-X	→	s-CX	Eley-Rideal mechanism when there is no barrier for reaction: s-H_2, s-CO and s-H_2CO
	→	s-C...X	Complex induced reaction mechanism otherwise: s-H_2O, s-CO_2, s-CH_3OH, s-CH_4 and s-NH_3
			Due to the large value of CH internal energy and because carbon atom complexes are characterized by short van der Waals distances (i.e. they should react easily), we consider that:
s-C...X + s-H	→	s-CHX	• most leads to more complex molecules (within a part will desorb due to reactive desorption),
	→	s-CH...X	• a small fraction remain on the form of s-CH...X (i.e. 1% in most cases),
	→	CH + s-X	• a small fraction of s-CH radicals desorb (i.e. 1%).
			The O...CO case:
s-O...CO + s-H	→	s-HOCO	• 19% lead to s-HOCO formation (within a part will desorb due to reactive desorption),
	→	s-OH + s-CO	• 20% of s-OH relaxation (much larger than for carbon atoms due to the larger van der Waals distance),
	→	s-H + s-CO_2	• 60% of s-CO_2 formation,
	→	OH + s-CO	• 1% of s-OH desorption.

ergized CH radicals are produced much closer to the molecule and should react more easily.

All the introduced processes and assumptions made are summarized in Table 1 and illustrated by the sketch of the Fig. 1.

2.2.2 *Formalism in the gas-grain code*

The Eley-Rideal and complexation mechanisms are computed assuming that for an incident species i and an adsorbed species j on the grain, the corresponding rate is given by:

$$R_{ij} = \eta_j \sigma_d \langle v(i) \rangle n(i) n_d \ \ [\mathrm{cm^{-3}s^{-1}}], \tag{3}$$

where $\eta_j = n_s(j)/\sum_k n_s(k)$ represents the average density of the molecule on the surface, σ_d the cross section of the grain, $\langle v(i) \rangle$ the thermal velocity of the incident species i, $n(i)$ its abundance and n_d the number density of grains. $n_s(k)$ refers to the surface abundance of the species k.

3 MODELING RESULTS

In the following sections, we present the results obtained with the new mechanisms introduced. For the simulations, we consider typical cold dense core conditions (Vasyunin & Herbst 2013) for our nominal model, i.e n_H=1.0 × 10^5 cm^{-3}, T_{gas}= T_{dust}=10K, A_V=10 and ζ_{H_2} = 1.3 × 10^{-17} s^{-1}. Initial input parameters and initial abundances are summarized in Tables 3 and 4. We first compare the nominal model (hereafter Model A) with Model B, which takes into account the mechanisms described in the previous section (i.e., carbon and oxygen complex induced reactions and the Eley-Rideal mechanism). We also considered an additional model in which we switched off the grain surface reaction s-H + s-CO → s-HCO in order to test our mechanism on the formation of methanol against the classical reaction scheme (Model C). We then performed a sensitivity analysis of our mechanism on the grain temperature, the cosmic ray ionization rate and the density.

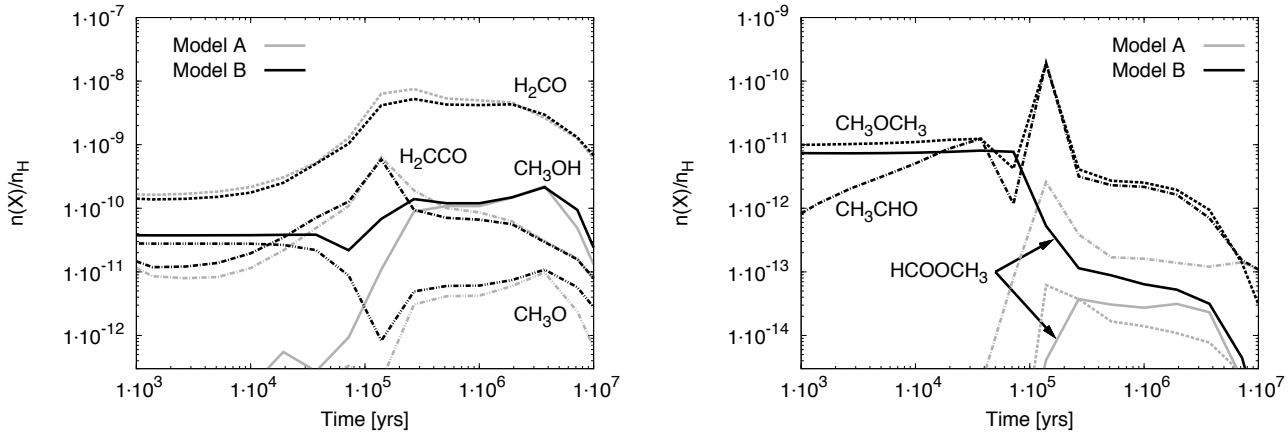

Figure 2. Abundance (with respect to n_H) of selected species in the gas-phase for Model A and B as a function of time.

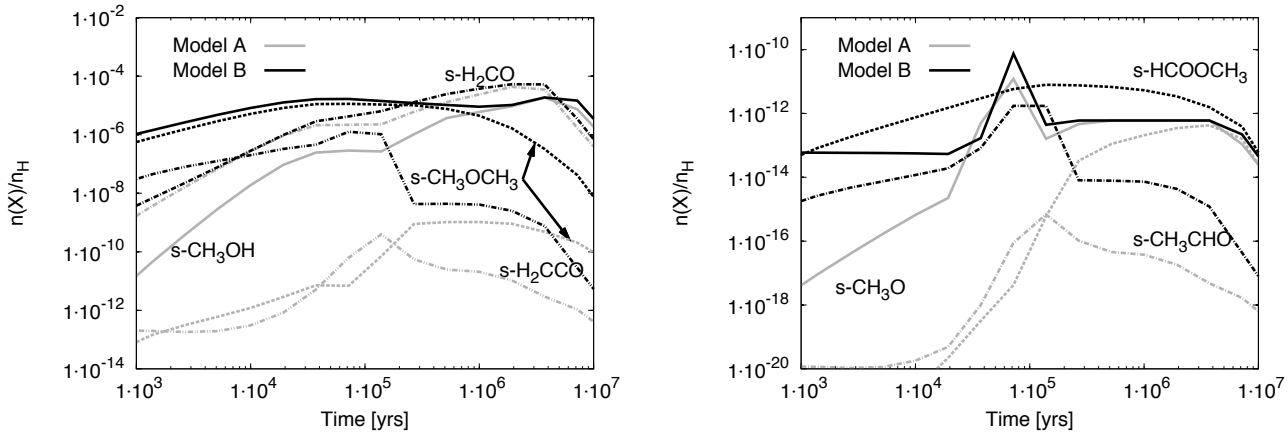

Figure 3. Abundance (with respect to n_H) of selected species on the grain surfaces for Model A and B as a function of time.

Table 2. Desorption energies of added species.

Species	E_D (K)	References
C...H_2O	3600	Schreiner & Reisenauer (2006)
C...NH_3	14400	Ab-initio calculations (this work)
C...CO_2	1200	M06-2X/cc-pVTZ (this work)
C...CH_4	400	Kim et al. (2003) (CCSD(T)/6-311+G(3df,2p))
C...CH_3OH	8400	Dede & Ozkan (2012)
O...CO	258	Goumans & Andersson (2010)
CH...H_2O	5800	Bergeat et al. (2009)
CH...NH_3	13470	Blitz et al. (2012)
CH...CO_2	1800	M06-2X/cc-pVTZ (this work)
CH...CH_3OH	5800	=CH...H_2O
CH_2...CO_2	1050	estimation
CH_3...CO_2	1175	estimation
CH_4...CO_2	1300	estimation
CH_3CO	2650	Garrod & Herbst (2006) (=CH_2CHO)
CH_3OCH_2	3500	estimation
CH_2NH_2	5530	Hama & Watanabe (2013) (=CH3OH)
CH_2NH	5530	Hama & Watanabe (2013) (=CH3OH)
HOCO	2000	Hama & Watanabe (2013) (/H_2CO)
HCOCO	2050	Hama & Watanabe (2013) (=H_2CO)
HCOCHO	2050	Hama & Watanabe (2013) (=H_2CO)
CH_3O	5084	Garrod & Herbst (2006) (=CH_2OH)

Table 3. Standard cold dense cloud model

Parameter	Value
T	10 K
n_H	1×10^5 cm^{-3}
A_V	10
ζ_{H_2}	1.3×10^{-17} s^{-1}
Initial abundances	Atomic (except for H)

3.1 Effect of the Eley-Rideal and complex induced reaction mechanisms

3.1.1 Formation of Complex Organic Molecules

Our calculations suggest that the Eley-Rideal and complex induced reaction mechanisms play an important role in the formation of some complex organic molecules. Figs. 2 and 3 show the abundances of a selection of these species (CH_3OH, H_2CO, H_2CCO, $HCOOCH_3$, CH_3OCH_3, CH_3CHO and CH_3O) as a function of time in the gas-phase and at the surface of the grains, for Models A (nominal model) and B (model with the new mechanisms). The H_2CO abundance is not changed in the gas-phase or on the grains. The H_2CCO abundance on the surface is strongly increased whereas in the gas it is unchanged. The gas phase abundances of H_2CO and H_2CCO do not change much because these species are

Table 4. Initial abundances used in our models.

Element	n_i/n_H [†]
H_2	0.5
He	0.09 [a]
N	6.2(-5) [b]
O	2.4(-4) [c]
C^+	1.7(-4) [b]
S^+	8.0(-9) [d]
Si^+	8.0(-9) [d]
Fe^+	3.0(-9) [d]
Na^+	2.0(-9) [d]
Mg^+	7.0(-9) [d]
P^+	2.0(-10) [d]
Cl^+	1.0(-9) [d]

[†] a(b) = a×10[b]
[a] See discussion in Wakelam & Herbst (2008)
[b] From Jenkins (2009)
[c] See discussion in Hincelin et al. (2011)
[d] Low metal abundance from Graedel et al. (1982)

efficiently produced in the gas phase following the forming process described in Vasyunin & Herbst (2013), i.e. O + CH_3 for H_2CO, O + C_2H_3 and the dissociative recombination of CH_3CO^+ for H_2CCO. For the other selected species, Model B shows a strong enhancement both in the gas-phase and at the surface of the grains.

Before 10^4 yr, carbon is mostly in atomic form (see Fig. 4). Thus the formation of C complexes with the main constituants of ices at these times, i.e. H_2O and CO, is very efficient and produces larger molecules more quickly than in Model A. The larger abundance of these species in the gas-phase then reflects the larger surface abundances.

In Model B, the formation of methanol starts on the surface by the formation of the s-C...H_2O complex through the adsorption of gas-phase atomic carbon on the water ice covered grain. The hydrogenation of this complex leads to a reorganization of the molecule to form s-CH_2OH and s-CH_3O. Hydrogenation of these molecules produce methanol:

$$\mathrm{C + s\text{-}H_2O \rightarrow s\text{-}C...H_2O \xrightarrow{s\text{-}H} s\text{-}CH_2OH/s\text{-}CH_3O \xrightarrow{s\text{-}H} s\text{-}CH_3OH} \quad (4)$$

Similarly, the CH_3OCH_3 molecule is formed on the surface through the following path:

$$\mathrm{C + s\text{-}CH_3OH \rightarrow s\text{-}C...CH_3OH \xrightarrow{s\text{-}H} s\text{-}CH_3OCH_2 \xrightarrow{s\text{-}H} s\text{-}CH_3OCH_3} \quad (5)$$

At early times, the s-CH_3OCH_3 abundance is increased because s-CH_3OH is more abundant and because the direct formation of s-C...CH_3OH by van der Waals complexes is more efficient than by a diffusive Langmuir-Hinshelwood mechanism.

The s-CH_3CHO molecule is formed by:

$$\mathrm{C + s\text{-}CO \rightarrow s\text{-}CCO \xrightarrow{s\text{-}H} s\text{-}HC_2O \xrightarrow{s\text{-}H} s\text{-}H_2CCO \xrightarrow{s\text{-}H} s\text{-}CH_3CO \xrightarrow{s\text{-}H} s\text{-}CH_3CHO.} \quad (6)$$

Here again, the s-CH_3CHO abundance is much larger compared to Model A because the precursor s-CCO is much more efficiently formed.

Although we did not change the formation of $HCOOCH_3$ on the surface, its abundance is strongly increased. In fact, during the formation of the COMs on the surface, a small fraction of the products (including intermediate radicals) desorb into the gas-phase due to reactive desorption. These radicals can then undergo gas-phase reactions and lead to the formation of more complex molecules (see also Vasyunin & Herbst 2013). Before 10^4 yr, $HCOOCH_3$ is formed by the reaction between atomic oxygen and CH_3OCH_2 (from reaction path (5)). After 10^4 yr, it is the dissociative recombination of $H_5C_2O_2^+$, itself formed from reaction between formaldehyde and $CH_3OH_2^+$, which produces $HCOOCH_3$.

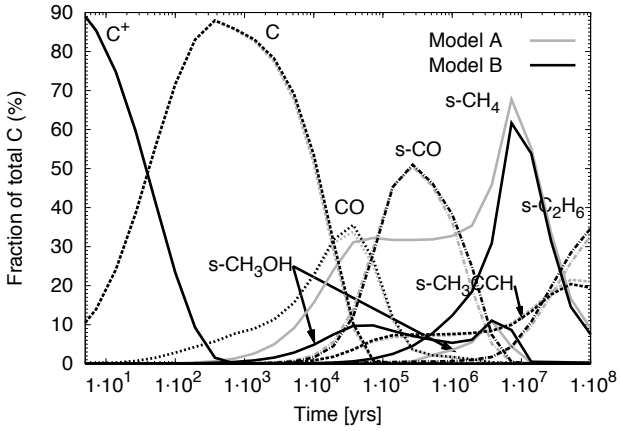

Figure 4. Main carriers of carbon as a function of time for Model A and B.

After a few 10^5 yr, other gas-phase reactions contribute to the formation of CH_3OCH_3 and CH_3CHO, such as the dissociative recombination of $CH_3OCH_4^+$ and CH_3CHOH^+ and the neutral-neutral reaction O + C_2H_5 → CH_3CHO + H. However, the formation paths (5) and (6) are always the dominant ones. It is interesting to point out that despite the fact that we have not changed the desorption mechanisms, the increase of the surface abundances are large enough to propagate to the gas-phase abundances. We have only considered a small efficiency for the chemical desorption (see section 2.1). Increasing this efficiency, would increase the gas-phase abundances of COMs by the same amount. Moreover, we have introduced the reactions of carbon atoms with H_2CO and CH_3CHO (as well as with CH_3OCH_3 and H_2CCO) using Husain & Ioannou (1999). These new reactions are rapid and decrease the abundance of these species as long as gas phase C is abundant (few 10^5 yr).

3.1.2 Effect on the major ice compounds

Figure 5 shows the abundances of the major ice compounds as a function of time for Models A and B. As expected the major ice component is water, with a fractional abundance $\geqslant 10^{-4}$ after 10^6 yr, which corresponds to approximately 100 monolayers deposited on each grain. CO becomes the second major component between 8×10^4 and 1×10^6 yr due to a massive freeze-out from the gas at these times. The modification of the chemical networks in Model B has a moderate impact on the ice composition compared to our nominal version except for s-CH_4 and s-CH_3OH.

The s-CH_3OH abundance is enhanced by several orders of magnitude until 2×10^6 yr, where both models give similar abundances. This difference is due to the efficient formation mechanism of s-CH_3OH through successive hydrogenation of s-C...H_2O as described before. In contrast s-CH_4 is strongly decreased until 5×10^6 years. This trend can be explained by the difference in the s-CH abundance, s-CH_4 being produced by the hydrogenation of s-CH in both models. In the new network, s-CH is formed by one of the product channels of the reactions between atomic hydrogen s-H and

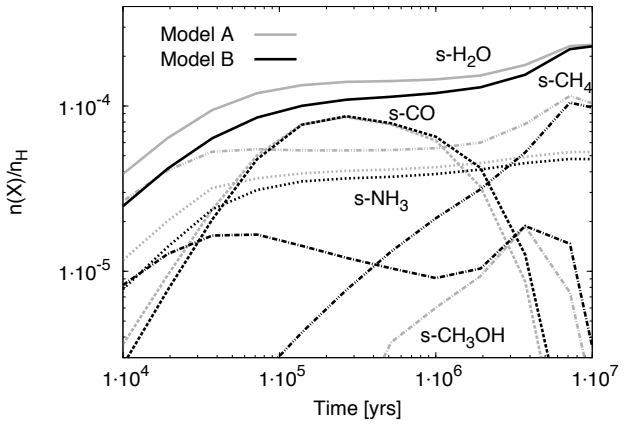

Figure 5. Major ice compounds abundance as a function of time for Models A and B.

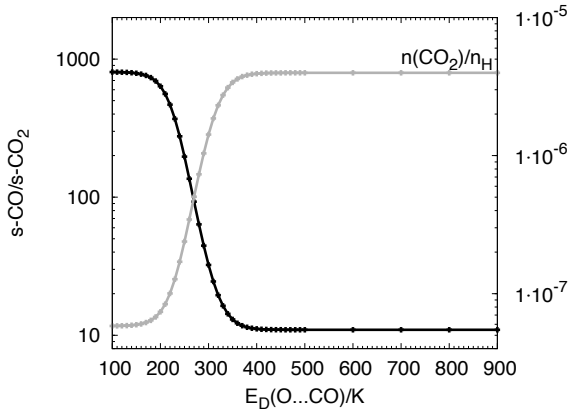

Figure 6. Computed s-CO/s-CO_2 ratio (at 10^6 yr) and CO_2 abundance on the grain surface as a function of the binding energy of s-O...CO(K).

complexes with atomic carbon (s-C...H_2O, s-C...NH_3, s-C...CO_2 etc, see Table A1 of Appendix A). The branching ratio producing s-CH for such channels have been set to 1% (see section 2.2.1). The consequence is that most of the carbon is then transferred into more complex species and the abundance of s-CH is much smaller compared to Model A, in which s-CH comes from the sticking of gas-phase CH. As a test, we have increased this branching ratio and the result is that the s-CH_4 increases until it produces the same amount of s-CH_4 as in Model A if the branching ratio is set to 100%.

3.1.3 The CO_2 ice case

Carbon dioxide is one of the most abundant species observed in interstellar ices ranging into the tens of percent with respect to the water ice abundance (see Öberg et al. 2011). Chemical models have difficulties to reproduce such large abundances of a species that need heavy species to diffuse on the cold interstellar grains before forming CO_2. Indeed, three processes are typically cited for the formation of CO_2 on grain surfaces (see Garrod & Pauly 2011):

$$\text{s-HCO} + \text{s-O} \rightarrow \text{s-CO}_2 + \text{H}, \quad (7)$$

$$\text{s-CO} + \text{s-OH} \rightarrow \text{s-CO}_2 + \text{H}, \quad (8)$$

$$\text{s-CO} + \text{s-O} \rightarrow \text{s-CO}_2. \quad (9)$$

Reaction (7) is barrierless but s-HCO is quickly hydrogenated to form s-H_2CO. Reaction (8) is typically assigned a small activation energy barrier but s-CO and s-OH need to be mobile on the grain surface, which is not the case at 10K considering diffusion by thermal hopping only. Reaction (9) is thought to require a more substantial activation energy (i.e. 1000K) but it happens to be the main formation path of CO_2 ice in Model A. Following Garrod & Pauly (2011) a new path is introduced in Model B:

$$\text{O} + \text{s-CO} \rightarrow \text{s-O...CO} \xrightarrow{\text{s-H}} \text{s-OH...CO} \rightarrow \text{s-CO}_2 + \text{s-H} \quad (10)$$

The efficiency of this formation mechanism depends on the binding energy of the s-O...CO complex. In Model B, we have assumed a value of 258 K based on Goumans & Andersson (2010). This value is calculated at the MPWB1K and CCSD(T)/CBS levels, which are thought to describe weak interactions well. However the calculations concern free CO and the binding value can be notably different for CO adsorbed on ice. To illustrate the effect of this assumption, we have varied this binding energy over the range 100-900 K. Fig. 6 presents the computed s-CO/s-CO_2 ratio as a function of E_D(s-O...CO) for t=10^6 yr. The efficiency of the conversion of s-CO to s-CO_2 strongly decreases with the binding energy of the s-O...CO complex and reaches a plateau when E_D(s-O...CO) is larger than 350 K. When the binding energy of s-O...CO is smaller than ≃200K, the life time of the s-O...CO complex on the grain surface is too short due to thermal evaporation and the complex is destroyed before reacting (i.e. for the set of parameters chosen here). When E_D≃350K, the oxygen is strongly bound to the CO and the life time of the O...CO complex on the grain surface is sufficiently long to form efficiently s-CO_2 by the introduced pathway (s-CO/s-CO_2≃10). In term of grain coverage, when E_D(s-O...CO)≳400K ∼ 2 monolayer of CO_2 ice are built on the grain surface.

3.2 Sensitivity to the model physical parameters

In this section, we study the sensitivity of our new model to the temperature, the cosmic ray ionization rate and the density.

3.2.1 Sensitivity to the temperature and the cosmic ray ionization rate

We have run Models A and B with a temperature of T=8 and 12 K (smaller and larger than in our nominal one) and for a cosmic ionization rate $\zeta_{H_2} = 5.0 \times 10^{-18}$ and 5.0×10^{-17} s^{-1} (again smaller and larger than the nominal model). For each model, all the other input parameters are kept constant and equal to the standard ones defined in Tables 3 and 4.

With a lower temperature (8K instead of 10 K), the abundances of methanol and the methoxy radical (CH_3O) are lowered by a factor of ∼ 10 between t=10^5 and 10^6 yr in the gas phase. At this temperature, the diffusion of atomic hydrogen is much less efficient than in the T=10 K case. This result is independent of the new mechanisms that we have introduced. At a temperature of 12 K instead of 10 K, the species abundances are not significantly affected, very likely because the increase of the surface reactivity is counterbalanced by the increase in the evaporation of atomic hydrogen from the surface.

Varying the cosmic ionization rate has a significant impact on the computed abundances of all the studied species. In particular, an increase in this rate increases the formation of radicals at

the surface of the grains by cosmic-ray induced UV photodissociations and increases the evaporation of surface species through the stochastic heating of grains. In our case, this promotes the surface radical coverage and helps to desorb molecules into the gas-phase. On average, the gas phase abundance of the studied species is enhanced by a factor of ∼2-10 between 10^5 and 10^6 yrs when ζ_{H_2} increases from 5.0×10^{-18} to 5.0×10^{-17} s^{-1}. This result was however also obtained with the older chemical network (Model A).

3.2.2 Sensitivity to the density

We ran Models A and B for densities n_H=1.0×10^4 and 1.0×10^6 cm^{-3}, in addition to the standard density of n_H=1.0×10^5 cm^{-3}. All the other input parameters were kept constant and equal to the standard ones defined in Tables 3 and 4. Fig. 7 shows the abundances of CH_3OH, CH_3O, H_2CCO and H_2CO in the gas-phase as a function of time for Model B and the three densities. In the gas-phase, as well on the grain surface, the abundance of these species rise earlier. This is due to a larger depletion of species onto the grains and thus a greater production of COMs. However, in the gas-phase, the abundance reach a plateau (similar for all densities) while the abundance on the grain surface is still increasing. This is due to the increase of the destruction by reactions with gas-phase atomic carbon (which is the main destruction path until carbon is in atomic form) with the density. This effect is only seen in Model B since with the introduced mechanisms the formation of COMs at early times is completely controlled by the abundance of gas-phase atomic carbon. At longer times ($\leqslant 10^5$ yr), the abundances are larger when the density is smaller simply because the species tend to stay on the grains at larger densities.

3.3 Sensitivity to the reaction s-CO + s-H

The efficiency of the formation of methanol on the surface by hydrogenation of CO ice is highly debated and there is still no real consensus. Initially Tielens & Hagen (1982) and Tielens & Allamandola (1987) proposed the following hydrogenation scheme from CO to CH_3OH (see Tielens & Charnley 1997):

$$\text{s-CO} \xrightarrow{\text{s-H}} \text{s-HCO} \xrightarrow{\text{s-H}} \text{s-H}_2\text{CO} \xrightarrow{\text{s-H}} \text{s-CH}_3\text{O} \xrightarrow{\text{s-H}} \text{s-CH}_3\text{OH},$$

Following this idea, several experimental studies of H-atom bombardment of CO ice were performed by different groups leading to conflicting results (Hiraoka et al. 2002; Watanabe & Kouchi 2002). Both, H + CO and H + H_2CO reactions, show notable barriers for reaction in the gas-phase and this is very likely to be the case on grain surfaces. However, on grain surfaces, H is expected to undergo efficient quantum tunneling. Fuchs et al. (2009) found that the discrepancy between these two groups was caused mainly by a difference in the H atom flux setting. They also found that the s-CO + s-H and s-H_2CO + s-H hydrogenation reactions proceed by a tunneling process with an energy barrier of 390 ± 40K and 415 ± 40K respectively (experience performed with a 12K interstellar ice analog).

In order to test this methanol formation path against our new mechanism, we ran an additional model in which we switched off the reaction s-CO + s-H in our Model B (i.e. which is equivalent to making the assumption that the thickness of the barrier cannot be overcome by tunneling). Fig. 8 shows the computed abundances of s-CO, s-HCO and s-CH_3OH for Model B and the additional model where the Eley-rideal and complex induced reactions mechanisms were allowed and the s-H + s-CO reaction turned off (Model C). Before 10^5yr, all computed abundances are similar in both models. After 10^5 yr, removing the hydrogenation of s-CO (Model C) increases strongly the abundance of s-CO. The abundance of CH_3OH in the gas-phase and on the grain surfaces is not too affected until ∼ 10^6 yr. As a conclusion, the new formation path of s-CH_3OH that we have introduced is found to be the dominant one until ∼ 10^6 yr and is able to produce a large amount of methanol on grain surfaces and in the gas-phase.

4 COMPARISON WITH OBSERVATIONS IN COLD DENSE CORES

To compare the modeling results with observations, we used the method described in Loison et al. (2014). We have computed at each time step the mean distance of disagreement using the following formula:

$$D(t) = \frac{1}{N_{obs}} \sum_i \mid log[n(X)_i(t)] - log[n(X)_{obs}] \mid, \qquad (11)$$

where $n(X)_i(t)$ is the calculated abundance of species i and $n(X)_{obs}$ the observed one. N_{obs} refers to the total number of observed species. With this method, the smaller the D value, the better the agreement between modeled and observed abundances.

In order to validate our introduced mechanism, we compared our modeling results with observations of the TMC-1 and L134N dark clouds for which many observational constraints are available (approximately 50 molecules for L134N and 60 for TMC-1 (see Agúndez & Wakelam 2013, for a review)). We ran models A and B with a density of $n_H = 2 \times 10^4$ cm^{-3}, all the other parameters being equal to those of Tables 3 and 4. We found a similar level of agreement between Model A and Model B with a "best age", using equation (11), of 2×10^6 yr and 1×10^6 yr for for TMC-1 and L134N respectively. At these times, and assuming that the observed abundances were reproduced by the model when the difference between the two was smaller than one order of magnitude, the fraction of reproduced molecule is ∼ 60 and ∼ 70% for TMC-1 and L134N respectively. The fact that both Models A and B produce similar agreements is due to the fact that the introduced mechanism does not greatly affect the molecules observed in these two clouds.

4.1 COMs in the TMC-1 dark cloud

Using the data from the 8 GHz to 50 GHz spectral survey of TMC-1 obtained with the 45m Nobeyama radiotelescope (Kaifu et al. 2004) we determined observational upper limits for CH_3OCH_3, CH_3NH_2 and $HCOOCH_3$. For this, the published noise values for each individual line of the survey were interpolated to create a regular noise vector spanning the observed frequency range. We used the WEEDS package (Maret et al. 2011) to create synthetic LTE spectra with the following common characteristics: a FWHM linewidth of Δ_v = 0.5 km.s^{-1} and an excitation temperature of T_{ex} =5 K. The column density of each modeled species was varied until at least one of the modeled lines had a peak temperature larger than three times the local noise value. Along with a fixed N(H_2)=10^{22} cm^{-2} this defines the upper limit on the abundance of each species. We find that N(CH_3OCH_3)/N(H_2) < 2×10^{-9}, N(CH_3NH_2)/N(H_2) < 5×10^{-9} and N($HCOOCH_3$)/N(H_2) < 1×10^{-9}. The calculated abundances of these species at the time of "best age" (i.e. determined in the previous section) with Model B (using a density of $n_H = 2 \times 10^4$) gives n(CH_3OCH_3)/n(H_2) = 8.30×10^{-12}, n(CH_3NH_2)/n(H_2) = 3.60×10^{-10} and n($HCOOCH_3$)/n(H_2) = 3.00×

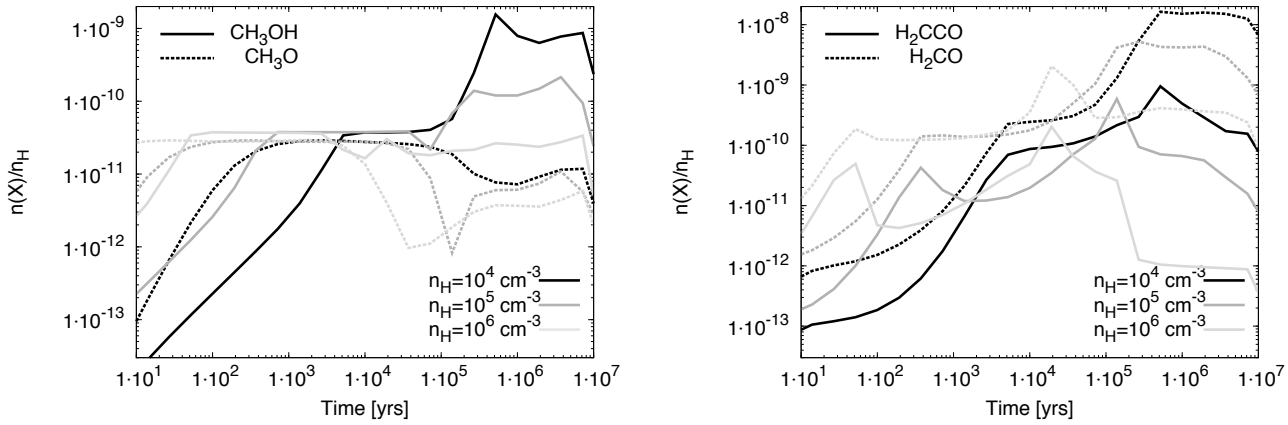

Figure 7. Abundance (with respect to n_H) as a function of time of selected gas-phase species for Model B with n_H=1.0 × 10^4, 1.0 × 10^5 and 1.0 × 10^6 cm^{-3}.

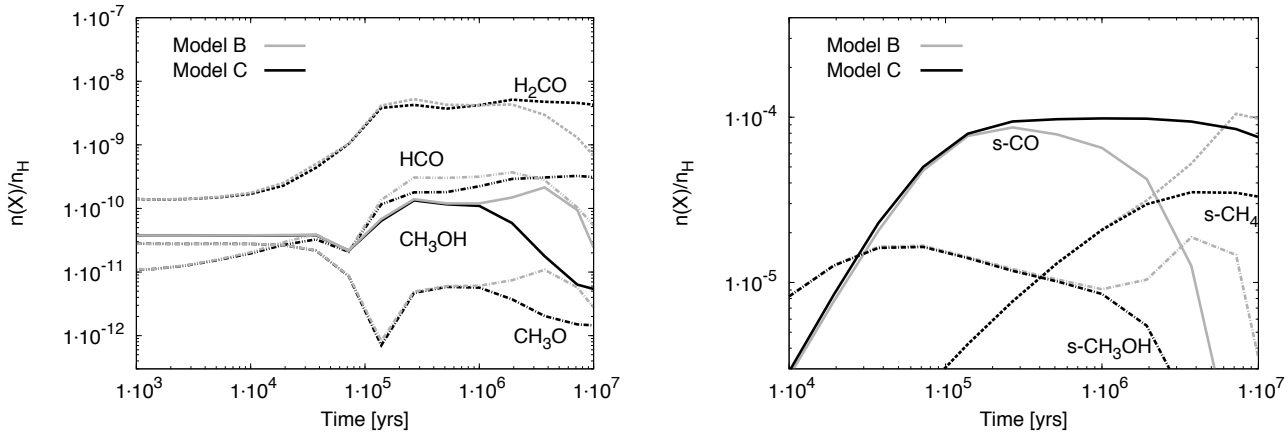

Figure 8. Abundance (with respect to n_H) as a function of time of selected gas-phase and grain surface species for Model B and C. Models ran using standard parameters defined in Tables 3 and 4.

10^{-13} which is far lower than the upper limits determined. These upper limits are therefore only poor constraints on the calculated COM abundances in this source.

In the two next sections, we focus on other dense cold sources where COMs have been observed.

4.2 L1689b and B1-b cold dense cores

In Table 5 we reported the observed COM abundances in B1-b and L1689b from Bacmann et al. (2012) and Cernicharo et al. (2012), together with the modeled abundances at the "best age". The modeled abundances have been obtained with Model A and B for a density of n_H=1.0 × 10^5 cm^{-3}. The "best age" was obtained by computing the distance of disagreement as previously explained and using the molecules listed in Table 5. We found the "best age" to be ∼ 1.0 × 10^5 yrs for L1689b and ∼ 5.0 × 10^5 for B1-b.

At the time of best agreement and except for $HCOOCH_3$, most of the computed abundances differ from observational abundances by less than a factor of ∼ 10 for all species when the Eley-Rideal mechanism and complex induced reactions are included (Model B). In the case of L1689b dense core, the observed abundances of CH_3OCH_3, CH_3CHO and H_2CCO are reproduced within a factor of 3 whereas H_2CO is reproduced within a factor of 8. In the case of B1-b dense core, CH_3O, CH_3OCH_3 and CH_3CHO are very well reproduced (within a factor of 3). H_2CCO and H_2CO are overproduced by a factor of ∼10 and ∼20 respectively while CH_3OH is underestimated by a factor of ∼10. For both clouds, Model B reproduces the observed COM abundances much better. Despite the fact that the $HCOOCH_3$ abundance is larger in Model B than in Model A, we still underestimate the abundance compared to the observations.

4.3 The prestellar core L1544

Recently, Vastel et al. (2014) reported the detection of a number of COMs in the prestellar core L1544. They estimate, thanks to the methanol lines, that these COM emissions come from the border of the core, at a radius of ∼ 8000 au, where T ∼ 10 K and n_{H_2} ∼ 2.0 × 10^4 cm^{-3}. In this region, Caselli et al. (2012) also revealed a large amount of water in the gas phase (i.e. $n(H_2O)/n_{H_2} \simeq 3.0\times10^{-7}$). The observed and computed abundances for Model A and B (n_H was set to 4.0 × 10^4 $cm^{-3}$and all the other input parameters equal to those defined in Tables 3 and 4) are reported in Table 6. The "best age" was found to be ∼ 3.0 × 10^5 yrs in Model A and ∼ 2.0 × 10^5 yrs in Model B.

In this source also, the computed abundances show a reason-

Table 5. Observed and computed fractional abundances of Complex Organic Molecules in L1689b and B1-b dense cores

	L1689b†	Model A	Model B	B1-b†	Model A	Model B
Density (in cm^{-3})		1×10^5	1×10^5		1×10^5	1×10^5
Time of best fit (in yrs)		2×10^5	2×10^5		5×10^5	5×10^5
$HCOOCH_3$	7.4(-10)	5.20(-14)	3.60(-13)	2.0(-11)	6.10(-14)	1.70(-13)
CH_3OCH_3	1.3(-10)	2.20(-13)	**2.35(-10)**	2.0(-11)	3.30(-14)	**5.50(-12)**
CH_3CHO	1.7(-10)	1.89(-12)	**1.80(-10)**	1.0(-11)	3.40(-13)	**4.70(-12)**
H_2CCO	2.0(-10)	**6.80(-10)**	**5.50(-10)**	1.3(-11)	2.00(-10)	1.40(-10)
CH_3O	...	2.90(-12)	7.55(-12)	4.7(-12)	**8.30(-12)**	**1.20(-11)**
H_2CO	1.3(-9)	1.60(-8)	1.05(-8)	4.0(-10)	1.05(-8)	8.50(-9)
CH_3OH	...	1.00(-10)	3.10(-10)	3.1(-9)	2.15(-10)	2.40(-10)

Observed and calculated fractional abundances expressed in unit of $n(X)/n(H_2)$. † Observed fractional abundances are those listed in Vasyunin & Herbst (2013). Boldface indicate less than a factor of 4 disagreement between model and observations. Here, a(b) stands for $a \times 10^b$.

Table 6. Observed and computed fractional abundance of Complex Organic Molecules in L1544 prestellar core

	L1544†	Model A	Model B
Density (in cm^{-3})		4×10^4	4×10^4
Time of best fit (in yrs)		3×10^5	2×10^5
$HCOOCH_3$	⩽1.5(-9)	2.20(-13)	4.15(-12)
CH_3OCH_3	⩽2.0(-10)	2.25(-13)	6.15(-11)
CH_3CHO	1.0(-10)	4.15(-12)	**6.65(-11)**
HCOOH	1.0(-10)	**2.25(-10)**	**3.75(-10)**
H_2CCO	1.0(-9)	**1.50(-9)**	**1.45(-9)**
CH_3CCH	5.0(-9)	9.20(-10)	8.40(-10)
CH_3O	⩽1.5(-10)	6.90(-12)	3.40(-12)
CH_3OH	6.0(-9)	4.65(-10)	3.60(-10)
H_2O	3.0(-7)	**9.40(-8)**	**3.20(-7)**

Observed and calculated fractional abundances expressed in unit of $n(X)/n(H_2)$. † Fractional abundances are from Vastel et al. (2014). Boldface indicate less than a factor of 4 disagreement between model and observations. Here, a(b) stands for $a \times 10^b$.

able agreement with the observed ones. In particular the abundances of HCOOH, H_2CCO, CH_3CHO and H_2O are very well reproduced (by less than a factor of 4 between the observed and the calculated abundances). However, we underestimate the abundance of CH_3OH and CH_3CCH by a factor of ~ 17, ~ 6 respectively. Our model predicts an abundance of $HCOOCH_3$, CH_3OCH_3 and CH_3O of 4×10^{-12}, 6×10^{-11} and 3×10^{-12} respectively.

It is very interesting to note that we do not need the photodesorption process, as suggested by the authors, to reproduce the observed COM and water abundances. In our case, the non-thermal desorption process is driven by a chemical desorption efficiency of 1%. This value is found to be sufficient to reproduce the observed gas phase abundances thanks to efficient COM and precursor formation on grain surfaces.

5 CONCLUSION

In this paper, we have studied the effect of the Eley-Rideal and complex induced reaction mechanisms of carbon atoms with the main ice components of dust grains on the formation of COMs in cold dense regions. This study was achieved using our gas-grain chemical model NAUTILUS. We used a moderate value for the efficiency of the chemical desorption (i.e. we considered that ∼1% of the newly formed species dessorb) in agreement with recent experiments made by Minissale & Dulieu (2014). We also studied the effect of oxygen complexation on CO ice on the formation of CO_2 ices.

The main conclusions of this modeling study can be summarized as follows:

(1) The Eley-Rideal and complex induced reaction mechanisms are found to enhance considerably the abundance of the most complex COMs both in the gas-phase and at the surface of grains. At the time of best agreement, we found that the gas-phase abundances of CH_3CHO, CH_3OCH_3 and $HCOOCH_3$ are enhanced at least by a factor ~ 10 up to ~ 100 when the Eley-Rideal and complex induced reaction mechanisms were activated while the abundances of H_2CO, CH_3O, CH_3OH and H_2CCO remains relatively constant. We find that using a moderate value of 1% for the chemical desorption efficiency, the surface abundances of complex species are large enough to propagate to the gas-phase abundances. The observed and calculated abundances of COMs in the different environments studied here are, in most cases, in good agreement.

(2) During this efficient production of COMs on grain surfaces, a small fraction of intermediate radicals are injected into the gas-phase. These intermediate radicals can then undergo gas-phase reactions and contribute to the formation of COMs in the gas-phase. These contributions are found to be efficient at evolved ages (i.e. when the carbon is mostly in molecular form). However, in most cases, the grain surface formation paths are found to be the dominant ones.

(3) We introduced the complex s-O...CO for the formation of CO_2 ice on grain surfaces. We assumed a binding energy of the s-O...CO complex of 258K based on Goumans & Andersson (2010). Using this value, the expected abundance of CO_2 ice is not achieved. This is due to the short lifetime of the s-O...CO complex on the grain surfaces (i.e. the complex is destroyed before reacting). We then studied the dependance of the CO/CO_2 ice ratios by varying the value of the binding energy of the s-O...CO complex. We find that a value of $E_D \approx 400$ K is sufficient to have a significant fraction of CO_2 ice on the grain surfaces (i.e. s-CO/s-$CO_2 \approx 10$).

(4) We observe that the main formation route to CH_3O is controlled by the grain surface reactions s-C...H_2O + s-H and s-H_2CO + s-H. These channels are sufficient enough to reproduce the observed abundance of the methoxy radical. In our models the proposed gas-phase formation route $CH_3OH + OH \rightarrow CH_3O + H_2O$ made by Cernicharo et al. (2012) and Vasyunin & Herbst (2013) is inefficient compared to those mentioned above.

(5) The methanol formation route by successive hydrogenation of the s-C...H_2O complex is found to be more competitive than the one usually proposed (i.e. by successive hydrogenation of s-CO) until $\sim 10^6$ yrs. The introduced reaction path is able to produce a

large amount of grain surface and gas-phase methanol. However, in all our models, we still underestimate the gas-phase methanol abundance at least by a factor of ~ 10 compared with the observations.

ACKNOWLEDGMENTS

MR, JCL, KMH, PG, FH and VW thanks the following funding agencies for their partial support of this work: the French CNRS/INSU programme PCMI and the ERC Starting Grant (3DICE, grant agreement 336474).

REFERENCES

Agúndez M., Wakelam V., 2013, Chemical Reviews, 113, 8710
Anicich V. G., 1993, Journal of Physical and Chemical Reference Data, 22, 1469
Arasa C., van Hemert M. C., van Dishoeck E. F., Kroes G. J., 2013, Journal of Physical Chemistry A, 117, 7064
Atkinson R., Baulch D. L., Cox R. A., Crowley J. N., Hampson R. F., Hynes R. G., Jenkin M. E., Rossi M. J., Troe J., 2004, Atmospheric Chemistry and Physics, 4, 1461
Bacmann A., Taquet V., Faure A., Kahane C., Ceccarelli C., 2012, A&A, 541, L12
Baulch D. L., Bowman C. T., Cobos C. J., Cox R. A., Just T., Kerr J. A., Pilling M. J., Stocker D., Troe J., Tsang W., Walker R. W., Warnatz J., 2005, Journal of Physical and Chemical Reference Data, 34, 757
Bergeat A., Moisan S., Mreau R., Loison J., 2009, Chemical Physics Letters, 480, 21
Blake G. A., Sutton E. C., Masson C. R., Phillips T. G., 1987, ApJ, 315, 621
Blitz M. A., Talbi D., Seakins P. W., Smith I. W. M., 2012, The Journal of Physical Chemistry A, 116, 5877
Bocherel P., Herbert L. B., Rowe B. R., Sims I. R., Smith I. W. M., Travers D., 1996, The Journal of Physical Chemistry, 100, 3063
Bottinelli S., Ceccarelli C., Neri R., Williams J. P., Caux E., Cazaux S., Lefloch B., Maret S., Tielens A. G. G. M., 2004, ApJL, 617, L69
Bromley S. T., Goumans T. P. M., Herbst E., Jones A. P., Slater B., 2014, Phys. Chem. Chem. Phys.
Canosa A., Sims I. R., Travers D., Smith I. W. M., Rowe B. R., 1997, A&A, 323, 644
Caselli P., Keto E., Bergin E. A., Tafalla M., Aikawa Y., Douglas T., Pagani L., Yíldíz U. A., van der Tak F. F. S., Walmsley C. M., Codella C., Nisini B., Kristensen L. E., van Dishoeck E. F., 2012, ApJL, 759, L37
Cernicharo J., Marcelino N., Roueff E., Gerin M., Jiménez-Escobar A., Muñoz Caro G. M., 2012, ApJL, 759, L43
Chang Y.-W., Wang N. S., 1995, Chemical Physics, 200, 431
Cohen N., Westberg K. R., 1991, Journal of Physical and Chemical Reference Data, 20
Cummins S. E., Linke R. A., Thaddeus P., 1986, ApJS, 60, 819
Cuppen H. M., Herbst E., 2007, ApJ, 668, 294
Dede Y., Ozkan I., 2012, Phys. Chem. Chem. Phys., 14, 2326
Dibble T. S., Zeng Y., 2010, Chemical Physics Letters, 495, 170
Dobe S., Berces T., Szilagyi I., 1991, J. Chem. Soc., Faraday Trans., 87, 2331
Fleurat-Lessard P., Rayez J.-C., Bergeat A., Loison J.-C., 2002, Chemical Physics, 279, 87
Friberg P., Hjalmarson A., Madden S. C., Irvine W. M., 1988, A&A, 195, 281
Fuchs G. W., Cuppen H. M., Ioppolo S., Romanzin C., Bisschop S. E., Andersson S., van Dishoeck E. F., Linnartz H., 2009, A&A, 505, 629
Fulle D., Hamann H. F., Hippler H., Troe J., 1996, The Journal of Chemical Physics, 105, 983
Garrod R. T., Herbst E., 2006, A&A, 457, 927
Garrod R. T., Pauly T., 2011, ApJ, 735, 15
Garrod R. T., Wakelam V., Herbst E., 2007, A&A, 467, 1103
Glass G. P., Kumaran S. S., Michael J. V., 2000, The Journal of Physical Chemistry A, 104, 8360
Goumans T. P. M., 2011, MNRAS, 413, 2615
Goumans T. P. M., Andersson S., 2010, MNRAS, 406, 2213
Graedel T. E., Langer W. D., Frerking M. A., 1982, ApJS, 48, 321
Grotheer H.-H., Rieketr G., Walter D., Just T., 1989, Symposium (International) on Combustion, 22, 963
Hama T., Watanabe N., 2013, Chemical Reviews, 113, 8783
Harding L. B., 1983, The Journal of Physical Chemistry, 87, 441
Harding L. B., Guadagnini R., Schatz G. C., 1993, The Journal of Physical Chemistry, 97, 5472
Harding L. B., Klippenstein S. J., Georgievskii Y., 2005, Proceedings of the Combustion Institute, 30, 985
Hasegawa T. I., Herbst E., 1993, MNRAS, 261, 83
Hasegawa T. I., Herbst E., Leung C. M., 1992, ApJS, 82, 167
Herbst E., van Dishoeck E. F., 2009, ARAA, 47, 427
Hickson K. M., Caubet P., Loison J.-C., 2013, The Journal of Physical Chemistry Letters, 4, 2843
Hincelin U., Chang Q., Herbst E., 2014, arXiv:1410.7375
Hincelin U., Wakelam V., Hersant F., Guilloteau S., Loison J. C., Honvault P., Troe J., 2011, A&A, 530, A61
Hippler H., Viskolcz B., 2002, Phys. Chem. Chem. Phys., 4, 4663
Hiraoka K., Sato T., Sato S., Sogoshi N., Yokoyama T., Takashima H., Kitagawa S., 2002, ApJ, 577, 265
Hoyermann K., Loftfield N., Sievert R., Wagner H., 1981, Symposium (International) on Combustion, 18, 831
Hoyermann K., Nacke F., 1996, Symposium (International) on Combustion, 26, 505
Husain D., Ioannou A. X., 1999, Journal of Photochemistry and Photobiology A: Chemistry, 129, 1
Husain D., Kirsch L. J., 1971, Trans. Faraday Soc., 67, 2025
Husain D., Young A., 1975, J. Chem. Soc., Faraday Trans. 2, 71, 525
Hwang D., Mebel A., Wang B., 1999, Chemical Physics, 244, 143
Jenkins E. B., 2009, ApJ, 700, 1299
Jimnez E., Gilles M., Ravishankara A., 2003, Journal of Photochemistry and Photobiology A: Chemistry, 157, 237
Johnson D. G., Blitz M. A., Seakins P. W., 2000, Phys. Chem. Chem. Phys., 2, 2549
Joshi A., Wang H., 2006, International Journal of Chemical Kinetics, 38, 57
Kaifu N., Ohishi M., Kawaguchi K., Saito S., Yamamoto S., Miyaji T., Miyazawa K., Ishikawa S.-I., Noumaru C., Harasawa S., Okuda M., Suzuki H., 2004, PASJ, 56, 69
Kim G.-S., Nguyen T. L., Mebel A. M., Lin S. H., Nguyen M. T., 2003, The Journal of Physical Chemistry A, 107, 1788
Loison J.-C., Halvick P., Bergeat A., Hickson K. M., Wakelam V., 2012, MNRAS, 421, 1476
Loison J.-C., Wakelam V., Hickson K. M., 2014, Monthly Notices of the Royal Astronomical Society, 443, 398
Loison J.-C., Wakelam V., Hickson K. M., Bergeat A., Mereau R., 2014, MNRAS, 437, 930

Maret S., Hily-Blant P., Pety J., Bardeau S., Reynier E., 2011, A&A, 526, A47
Matthews H. E., Friberg P., Irvine W. M., 1985, ApJ, 290, 609
Michael J. V., Nava D. F., Payne W. A., Stief L. J., 1979, The Journal of Chemical Physics, 70, 5222
Minissale M., Dulieu F., 2014, The Journal of Chemical Physics, 141,
Moskaleva L. V., Lin M. C., 1998, The Journal of Physical Chemistry A, 102, 4687
Nguyen T., Xue B., Weston R., Barker J., Stanton J., 2012, The Journal of Physical Chemistry Letters, 3, 1549
Öberg K. I., Boogert A. C. A., Pontoppidan K. M., van den Broek S., van Dishoeck E. F., Bottinelli S., Blake G. A., Evans II N. J., 2011, ApJ, 740, 109
Öberg K. I., Bottinelli S., Jørgensen J. K., van Dishoeck E. F., 2010, ApJ, 716, 825
Oehlers C., Wagner H. G., Ziemer H., Temps F., Db S., 2000, The Journal of Physical Chemistry A, 104, 10500
Ozkan I., Dede Y., 2012, Int. J. Quantum Chem., 112, 1165
Reboussin L., Wakelam V., Guilloteau S., Hersant F., 2014, MNRAS, 440, 3557
Röhrig M., Wagner H. G., 1994, Symposium (International) on Combustion, 25, 975
Sayah N., Li X., Caballero J., Jackson W., 1988, Journal of Photochemistry and Photobiology A: Chemistry, 45, 177
Schreiner P. R., Reisenauer H. P., 2006, ChemPhysChem, 7, 880
Seetula J., Kalinovski I., Slagle I., Gutman D., 1994, Chemical Physics Letters, 224, 533
Semenov D., Hersant F., Wakelam V., Dutrey A., Chapillon E., Guilloteau S., Henning T., Launhardt R., Piétu V., Schreyer K., 2010, A&A, 522, A42
Senosiain J. P., Klippenstein S. J., Miller J. A., 2006, The Journal of Physical Chemistry A, 110, 5772
Shannon R., Blitz M., Goddard A., Heard D., 2013, Nature Chemistry, pp 745–749
Song X., Hou H., Wang B., 2005, Phys. Chem. Chem. Phys., 7, 3980
Stief L. J., Nesbitt F. L., Payne W. A., Kuo S. C., Tao W., Klemm R. B., 1995, The Journal of Chemical Physics, 102, 5309
Talbi D., Chandler G., Rohl A., 2006, Chemical Physics, 320, 214
Talbi D., Smith I. W. M., 2009, Phys. Chem. Chem. Phys., 11, 8477
Tielens A. G. G. M., Allamandola L. J., 1987, in Hollenbach D. J., Thronson Jr. H. A., eds, Interstellar Processes Vol. 134 of Astrophysics and Space Science Library, Composition, structure, and chemistry of interstellar dust. pp 397–469
Tielens A. G. G. M., Charnley S. B., 1997, Origins of Life and Evolution of the Biosphere, 27, 23
Tielens A. G. G. M., Hagen W., 1982, A&A, 114, 245
Tsang W., 1987, Journal of Physical and Chemical Reference Data, 16, 471
Tsang W., Hampson R. F., 1986, Journal of Physical and Chemical Reference Data, 15, 1087
Vastel C., Ceccarelli C., Lefloch B., Bachiller R., 2014, ApJL, 795, L2
Vasyunin A. I., Herbst E., 2013, ApJ, 769, 34
Wakelam V., Herbst E., 2008, ApJ, 680, 371
Wakelam V., Herbst E., Loison J.-C., Smith I. W. M., Chandrasekaran V., Pavone B., Adams N. G., Bacchus-Montabonel M.-C., Bergeat A., Béroff K., Bierbaum V. M., Chabot M., Dalgarno A., van Dishoeck e. a., 2012, ApJS, 199, 21
Wakelam V., Smith I. W. M., Loison J.-C., Talbi D., Klippenstein S. J., Bergeat A., Geppert W. D., Hickson K. M., 2013, arXiv:1310.4350
Watanabe N., Kouchi A., 2002, ApJL, 571, L173
Woods P. M., Slater B., Raza Z., Viti S., Brown W. A., Burke D. J., 2013, ApJ, 777, 90
Xu S., Lin M., 2007, Proceedings of the Combustion Institute, 31, 159
Xu S., Zhu R. S., Lin M. C., 2006, International Journal of Chemical Kinetics, 38, 322
Yang Y., Zhang W., Pei S., Shao J., Huang W., Gao X., 2005, Journal of Molecular Structure: {THEOCHEM}, 725, 133
Yetter R. A., Rabitz H., Dryer F. L., Maki R. G., Klemm R. B., 1989, The Journal of Chemical Physics, 91, 4088
Yu H.-G., Francisco J. S., 2008, The Journal of Chemical Physics, 128,
Yu H.-G., Muckerman J. T., Francisco J. S., 2007, The Journal of Chemical Physics, 127,
Yu T., Yang D. L., Lin M. C., 1993, International Journal of Chemical Kinetics, 25, 1053
Zabarnick S., Fleming J., Lin M., 1988, Symposium (International) on Combustion, 21, 713

APPENDIX A: REACTIONS ADDED TO THE NETWORK

Table A1. Grain chemistry

Reaction			Barrier (K)	Branching ratios	Comments
Eley-Rideal and complex induced reaction mechanisms					
C + s-H_2O	→	s-C...H_2O	0		Ab-initio calculations
C + s-CO_2	→	s-C...CO_2	0		M06-2X/cc-pVTZ
C + s-NH_3	→	s-C...NH_3	0		Ab-initio calculations
C + s-CH_4	→	s-C...CH_4	0		Ab-initio calculations
C + s-CH_3OH	→	s-C...CH_3OH	0		Ab-initio calculations
CH + s-H_2O	→	s-CH...H_2O	0		Ab-initio calculations
CH + s-CO_2	→	s-CH...CO_2	0		Ab-initio calculations
CH + s-NH_3	→	s-CH...NH_3	0		Blitz et al. (2012)
CH + s-CH_3OH	→	s-CH...CH_3OH	0		Ab-initio calculations
O + s-CO	→	s-O...CO	0		Goumans & Andersson (2010); Talbi et al. (2006)
C + s-CO	→	s-CCO	0		Ab-initio calculations
C + s-H_2	→	s-CH_2	0		Husain & Kirsch (1971); Husain & Young (1975) Harding (1983); Harding et al. (1993)
C + s-H_2CO	→	s-H_2CCO	0		Husain & Ioannou (1999)
Grain surface reactions					
s-C...H_2O +s-H	→	s-CH_2OH	0	49%	
	→	s-CH_3O	0	49%	
	→	s-CH...H_2O	0	1%	
	→	CH + s-H_2O	0	1%	
s-C...NH_3 +s-H	→	s-CH_2NH_2	0	98%	
	→	s-CH...NH_3	0	1%	
	→	CH + s-NH_3	0	1%	
s-C...CO_2 + s-H	→	s-HC(O)CO	0	0%	
	→	s-HCO + s-CO	0	98%	
	→	s-CH...CO_2	0	1%	
	→	CH + s-CO_2	0	1%	
s-C...CH_4 +s-H	→	s-C_2H_5	0		Fleurat-Lessard et al. (2002)
s-C...CH_3OH +s-H	→	s-CH_3OCH_2	0	89%	
	→	s-CH...CH_3OH	0	10%	
	→	CH + s-CH_3OH	0	1%	
s-CH...H_2O + s-H	→	s-CH_2 + s-H_2O	0		Ab-initio calculations
s-CH...CO_2 + s-H	→	s-CH_2...CO_2	0		
s-CH_2...CO_2 + s-H	→	s-CH_3...CO_2	0		
s-CH_3...CO_2 + s-H	→	s-CH_4...CO_2	0		
s-CH...NH_3 + s-H	→	s-CH_2 + s-NH_3	0		
s-CH...CH_3OH + s-H	→	s-CH_2 + s-CH_3OH	0		
s-O...CO + s-H	→	s-HOCO	0	19%	Yu & Francisco (2008); Dibble & Zeng (2010)
	→	s-CO_2 + s-H	0	60%	Yu & Francisco (2008); Dibble & Zeng (2010)
	→	s-OH + s-CO	0	20%	Yu & Francisco (2008); Dibble & Zeng (2010)
	→	OH + s-CO	0	1%	
s-CH_3OCH_2 + s-H	→	s-CH_3OCH_3	0		Dimethyl ether formation
s-CH_2NH_2 + s-H	→	s-CH_3NH_2	0		Ab-initio calculations
s-C...NH_3 + s-N	→	s-HCN + s-NH_2	0		Talbi & Smith (2009)
s-HC(O)CO + s-H	→	s-HC(O)CHO	0		Glyoxal formation
s-CCO + s-H	→	s-HCCO	0		
s-HCCO + s-H	→	s-H_2CCO	0		
s-H_2CCO + s-H	→	s-CH_3CO	1720		Michael et al. (1979)
s-CH_3CO + s-H	→	s-CH_3CHO	0		
s-CH_3CO + s-CH_3	→	s-$CH_3C(O)CH_3$	0		Acetone formation
s-HOCO + s-H	→	s-HCOOH	0	10%	Yu & Francisco (2008); Dibble & Zeng (2010)
	→	s-CO_2 + s-H_2	0	70%	Yu & Francisco (2008); Dibble & Zeng (2010)
	→	s-H_2O + s-CO	0	20%	Yu & Francisco (2008); Dibble & Zeng (2010)
s-HOCO + s-N	→	s-OH + s-OCN	0	50%	Dibble & Zeng (2010)
	→	s-NH + s-CO_2	0	50%	Dibble & Zeng (2010)
s-HOCO + s-O	→	s-OH + s-CO_2	0		Yu et al. (2007)
s-OH + s-CO	→	s-HOCO	150		Fulle et al. (1996)
	→	s-CO_2 + s-H	150		Fulle et al. (1996)
s-H_2CO + s-H	→	s-CH_3O	2400		Hippler & Viskolcz (2002)
	→	s-CH_2OH	5400		Hippler & Viskolcz (2002)
	→	s-HCO + s-H_2	1740		Oehlers et al. (2000)
s-CH_3O + s-H	→	s-CH_3OH	0		
s-O + s-CH_3	→	s-CH_3O	0		
s-CH_3 + s-CH_3O	→	s-CH_3OCH_3	0		
s-HCO + s-CH_3O	→	s-$HCOOCH_3$	0		

Table A2. Gas phase reactions (temperature range is 10-300K).

Reaction			α^a	β^a	γ^a	$F_0{}^b$	g^c	Form.^{d}	Comments
$H + CH_2NH_2$	→	$CH_2NH + H_2$	3.0(-12)	0	0	3	0	1	Equal to $H + C_2H_5$
	→	$CH_3 + NH_2$	1.07(-10)	0	0	3	0		
$O + CH_2NH_2$	→	$CH_2NH + H_2$	1.0(-11)	0	0	2	0	1	/ $O + C_2H_5$ Harding et al. (2005)
	→	$H_2CO + NH_2$	1.0(-10)	0	0	2	0		/ $O + C_2H_5$ Tsang & Hampson (1986)
$C + CH_2NH_2$	→	$C_2H_2 + NH_2$	3.0(-10)	0	0	3	0	1	k / C + alkenes and products from Moskaleva & Lin (1998)
$N + CH_2NH_2$	→	$CH_2NH + NH$	4.0(-11)	0.17	0	2	7	1	/ $N + C_2H_5$ Stief et al. (1995); Yang et al. (2005)
	→	$HCN + NH_3$	6.0(-11)	0.17	0	3	21		
$H + CH_2OH$	→	$H_2CO + H_2$	1.0(-11)	0	0	2	0	1	Tsang (1987)
	→	$CH_3 + OH$	1.6(-10)	0	0	2	0		Tsang (1987)
$O + CH_2OH$	→	$H_2CO + OH$	1.0(-10)	0	0	2	0	1	Seetula et al. (1994); Grotheer et al. (1989)
$C + CH_2OH$	→	$CH_3 + CO$	3.0(-10)	0	0	3	0	1	k / C + alkenes and products from Senosiain et al. (2006)
$N + CH_2OH$	→	$H_2CO + NH$	4.0(-11)	0.17	0	2	7	1	/ $N + C_2H_5$ Stief et al. (1995); Yang et al. (2005)
	→	$HCN + H_2O$	6.0(-11)	0.17	0	3	21		
$H + CH_3O$	→	$H_2CO + H_2$	3.0(-11)	0	0	1.6	100	1	Hoyermann et al. (1981); Dobe et al. (1991)
	→	$CH_3 + OH$	3.0(-12)	0	0	1.6	100		
$O + CH_3O$	→	$H_2CO + OH$	6.0(-12)	0	0	1.8	100	1	Hoyermann et al. (1981); Dobe et al. (1991)
	→	$CH_3 + O_2$	1.9(-12)	0	0	1.8	100		
$C + CH_3O$	→	$CH_3 + CO$	3.0(-10)	0	0	3	0	1	k / C + alkenes and products from Senosiain et al. (2006)
$N + CH_3O$	→	$H_2CO + NH$	1.0(-11)	0.17	0	2	7		/ $N + C_2H_5$ Stief et al. (1995); Yang et al. (2005)
	→	$CH_3 + NO$	3.0(-11)	0.17	0	3	21	1	
$CN + CH_3OH$	→	$CH_3O + HCN$	6.0(-11)	0	0	3	0	1	Sayah et al. (1988)
	→	$CH_2OH + HCN$	6.0(-11)	0	0	3	0		Sayah et al. (1988)
$OH + CH_3OH$	→	$CH_3O + H_2O$	6.0(-13)	-1.2	0	2	10	1	Shannon et al. (2013)
	→	$CH_2OH + H_2O$	3.1(-12)	0	360	1.8	100		Atkinson et al. (2004)
$CH + CH_3OH$	→	$CH_3 + H_2CO$	2.5(-10)	0	0	1.6	10	1	Rate constant from Johnson et al. (2000)
$C + H_2CO$	→	$CH_2 + CO$	3.0(-10)	0	0	1.8	0	1	Husain & Ioannou (1999)
$CH + H_2CO$	→	$CH_3 + CO$	4.0(-10)	0	0	1.8	10	1	Zabarnick et al. (1988)
$CN + H_2CO$	→	$HCN + HCO$	1.0(-11)	-0.4	0	3	100	1	Yu et al. (1993); Chang & Wang (1995) assuming submerged barrier by comparison with $CN + C_2H_6$
$OH + H_2CO$	→	$H_2O + HCO$	1.0(-11)	-0.6	0	2	10	1	Xu et al. (2006)
$C + CH_3OCH_3$	→	$CH_3O + C_2H_4$	3.0(-10)	0	0	3	100	1	/ $C + CH_3OH$
$H + CH_3OCH_2$	→	$CH_3O + CH_3$	3.0(-11)	0	0	2	100	1	/ $H + CH_2OH$
$O + CH_3OCH_2$	→	$HCOOCH_3 + H$	2.56(-10)	0.15	0	1.6	10	1	Hoyermann & Nacke (1996); Song et al. (2005)
$N + CH_3OCH_2$	→	$CH_3O + H_2CN$	3.0(-11)	0	0	3	10	1	/ $N + C_2H_5$ Stief et al. (1995); Yang et al. (2005)
$C + CH_3OCH_2$	→	$CH_3O + C_2H_2$	3.0(-10)	0	0	3	10	1	Capture rate constant, various products possible
C + HCOOCH3	→	$2xCO + H + CH_3$	3.0(-10)	0	0	3	100	1	Capture rate constant, various products possible but CO is very likely produced
$H + HCCO$	→	$CH_2 + CO$	1.7(-10)	0	0	1.6	0	1	Glass et al. (2000); Baulch et al. (2005)
$C + HCCO$	→	$C_2H + CO$	2.0(-10)	0	0	3	0	1	Estimation
$O + HCCO$	→	$H + CO + CO$	1.6(-10)	0	0	1.6	0	1	Baulch et al. (2005)
	→	$CH + CO_2$	4.9(-11)	0	560	2	100		
$N + HCCO$	→	$HCN + CO$	6.0(-11)	0	0	3	10	1	Estimation, part of the HCN lead to
	→	$HNC + CO$	4.0(-11)	0	0	3	10		HNC considering the available energy
$C + CH_2CO$	→	$C_2H_2 + CO$	3.0(-10)	0	0	3	0	1	
$C + CH_3CHO$	→	$C_2H_4 + CO$	3.0(-10)	0	0	1.8	0	1	Husain & Ioannou (1999)
$HCCO + H_3^+$	→	$H_2CCO^+ + H_2$	1.0	3.1(-9)	2.8	3	0	2	Capture rate, this work
$HCCO + H_3O^+$	→	$H_2CCO^+ + H_2O$	1.0	1.4(-9)	2.8	3	0	2	Capture rate, this work
$HCCO + HCO^+$	→	$H_2CCO^+ + CO$	1.0	1.3(-9)	2.8	3	0	2	Capture rate, this work
$HCCO + N_2H^+$	→	$H_2CCO^+ + N_2$	1.0	1.3(-9)	2.8	3	0	2	Capture rate, this work
$H_2CCO^+ + H$	→	$CH_3^+ + CO$	1.0	1.94(-9)	0.0	3	0	3	Capture rate, this work
$CH_4^+ + CO$	→	$HCO^+ + CH_3$	1.0	7.6(-10)	0.28	2	0	3	Anicich (1993)

[a] α, β and γ are the parameters used to compute the rate of the reaction.
[b] F_0 is an uncertainty parameter.
[c] g is used to parametrize a possible temperature-dependence of the uncertainty F_0.
[d] Formula ton compute the temperature dependent rate coefficient: 1: $k(T_{gas})_{Kooij} = \alpha(T_{gas}/300)^{\beta} e^{-\gamma/T_{gas}}$, 2: $k(T_{gas})_{Ionpol1} = \alpha\beta(0.62 + 0.4767\gamma(300/T_{gas})^{0.5})$ 3: $k(T_{gas})_{Ionpol2} = \alpha\beta(1.0 + 0.0967\gamma(300/T_{gas})^{0.5} + (\gamma^2/10.526)(300/T_{gas}))$(see Wakelam et al. 2012, for more information).